Coordinate-Based Seismic Interpolation in Irregular Land Survey: A Deep Internal Learning Approach

Goyes-Peñafiel, Paul
Vargas, Edwin
Correa, Claudia V.
Sun, Yu
Kamilov, Ulugbek S.
Wohlberg, Brendt Egon
Arguello, Henry

To be published in: IEEE Transactions on Geoscience and Remote Sensing

DOI to publisher's version: 10.1109/TGRS.2023.3290468

Coordinate-Based Seismic Interpolation in Irregular Land Survey: A Deep Internal Learning Approach

Paul Goyes-Peñafiel, Edwin Vargas,
Claudia V. Correa, Yu Sun, Ulugbek S. Kamilov, Brendt Wohlberg, and Henry Arguello

***Abstract*— Physical and budget constraints often result in irregular sampling, which complicates accurate subsurface imaging. Preprocessing approaches, such as missing trace or shot interpolation, are typically employed to enhance seismic data in such cases. Recently, deep learning has been used to address the trace interpolation problem at the expense of large amounts of training data to adequately represent typical seismic events. Nonetheless, most research in this area has focused on trace reconstruction, with little attention having been devoted to shot interpolation. Furthermore, existing methods assume regularly spaced receivers/sources failing in approximating seismic data from real (irregular) surveys. This work presents a novel shot gather interpolation approach which uses a continuous coordinate-based representation of the acquired seismic wavefield parameterized by a neural network. The proposed unsupervised approach, which we call coordinate-based seismic interpolation (CoBSI), enables the prediction of specific seismic characteristics in irregular land surveys without using external data during neural network training. Experimental results on real and synthetic 3-D data validate the ability of the proposed method to estimate continuous smooth seismic events in the time-space and frequency-wavenumber domains, improving sparsity or low-rank-based interpolation methods.**

***Index Terms*— Deep internal learning, irregular land surveys, positional encodings, seismic shot interpolation.**

This work was supported in part by the project through the agreement 785-2019 between the Agencia Nacional de Hidrocarburos (ANH) and the Ministerio de Ciencia, Tecnología e Innovación (MINCIENCIAS) and Fondo Nacional de Financiamiento para la Ciencia, la Tecnología y la Innovación Francisco José de Caldas, under Grant 110287780575; and in part by the Laboratory Directed Research and Development Program of the Los Alamos National Laboratory under Project 20200061DR. *(Paul Goyes-Peñafiel and Edwin Vargas contributed equally to this work.) (Corresponding author: Henry Arguello.)*

Paul Goyes-Peñafiel, Claudia V. Correa, and Henry Arguello are with the Department of Computer Science, Universidad Industrial de Santander, Bucaramanga 680002, Colombia (e-mail: goyes.yesid@gmail.com; henarfu@uis.edu.co).

Edwin Vargas is with the Department of Electronics Engineering, Universidad Industrial de Santander, Bucaramanga 680002, Colombia.

Yu Sun was with the Department of Computer Science and Engineering, Washington University in St. Louis, St. Louis, MO 63130 USA. He is now with the Department of Computational and Mathematical Sciences, California Institute of Technology, Pasadena, CA 91125, USA.

Ulugbek S. Kamilov is with the Department of Electrical and System Engineering and the Department of Computer Science and Engineering, Washington University in St. Louis, St. Louis, MO 63130 USA.

Brendt Wohlberg is with Theoretical Division, Los Alamos National Laboratory, Los Alamos, NM 87545 USA.

I. Introduction

INTERPOLATION is of great importance within the seismic data processing workflow because environmental or topographic restrictions usually result in incomplete and irregular receiver and source sampling. Some limitations include natural and anthropological factors such as water bodies, and infrastructure, as well as equipment errors [1]. The most common seismic interpolation approach involves recovering missing traces of a shot gather. A more complex approach focuses on estimating complete missing shot gathers, entailing greater economic, environmental, and implementation benefits. Nonetheless, most of the work reported in the literature deals with trace interpolation, with limited consideration having been given to shot interpolation. Thus, this work focuses on interpolating missing seismic shots in irregularly sampled land surveys.

Shot interpolation has typically been addressed by convex optimization, aiming at inverting the acquisition model using a regularizer that imposes prior knowledge about the data such as sparsity in domains like wavelet, curvelet, shearlet, and learned dictionaries [2], [3], [4]. More recently [5], sparse regularization has been jointly integrated with implicit regularization provided by denoising algorithms using the plug and play priors and consensus equilibrium framework [6], [7], [8]. The versatility of deep learning has also been explored to solve the shot interpolation problem in a supervised fashion [9], specifically with a residual network architecture trained on data samples generated with bicubic interpolation of the incomplete dataset.

A key aspect of supervised deep learning approaches for seismic data interpolation is that they employ external datasets. For instance, a number of authors [10], [11], [12], [13], [14] employ convolutional neural networks (CNNs) following an end-to-end training strategy that requires large training datasets. Alternatively, deep internal learning approaches that exploit the structural redundancy of the field data itself, rather than employing vast training datasets, have been proposed for seismic trace interpolation [15], [16], using deep image priors (DIPs) [17], [18], [19] and recurrent neural networks (RNNs) [20]. Further, a combination of internal and external learning for trace interpolation has been studied [21]. Although all these works have explored deep learning-based solutions for irregular subsampling schemes [22], [23], they implicitly

require a binning process to rearrange irregularly sampled seismic data onto a regular grid with missing entries (traces).

In contrast, this work presents a deep internal learning approach to estimate complete missing shot gathers in an irregular land survey bypassing the binning step. The proposed method takes advantage of a recent branch of work in computer graphics, coordinate-based neural representations, which allows the encoding of a continuous spatial field into the weights of a multilayer perceptron (MLP) by mapping coordinates to pixel values, in an unsupervised manner [24], [25], [26]. Specifically, the proposed coordinate-based seismic interpolation (CoBSI) method learns a continuous mapping from the spatial and temporal coordinates of the (incomplete) acquired seismic data to the underlying recorded field. The continuous nature of the neural representation can model irregular sampling scenarios without a binning process and is not constrained to have a spatial resolution, reducing memory costs compared with discrete representations. Furthermore, in contrast to current state-of-the-art methods, the proposed approach enables seismic shot interpolation for both regular and irregular 3-D land surveys, in an unsupervised fashion, i.e., without additional training data. The proposed approach is validated using 3-D seismic data from orthogonal grids such as cross-spreads, focusing specially on randomly subsampled regular and irregular grids with acoustic synthetic data, *Stratton survey* [27] and *SEAM Phase II Foothills model* [28]. The results show that CoBSI outperforms the multichannel singular spectrum analysis (MSSA), damped-MSAA (DMSSA), sequential generalized K-means (SGK), and sparsity-based shot reconstruction methods.

II. Background

Coordinate-based neural representations have been successfully applied to unsupervised generation of highly realistic views of scenes with complicated geometries and appearance [26], [29], and implicit neural representations of signals for solving boundary value problems [25]. In the same line of work, the coordinate-based internal learning (CoIL) approach in [24] extrapolated these ideas to solve imaging inverse problems by modeling a continuous measurement field from a subsampled and noisy set of measurements, using geometry parameters of a tomographic imaging system. Since a seismic acquisition can be described in terms of a coordinate system, resembling the continuous field modeling from the computer vision area, this work explores a coordinate-based modeling to address the seismic shot interpolation problem in a deep internal learning approach. It is worth pointing out that CoBSI addresses a substantially more complex interpolation than that in [24], since the seismic wavefield we want to interpolate contains different responses from reflected, refracted, and surface waves.

This approach consists of two main processing blocks: a positional encoder and an MLP. The positional encoding maps help to preserve high-frequency information through the encoding of coordinate positions [30], while the MLP works as an interpolator from the encoded coordinates to the signal amplitude. For instance, Tancik et al. [29] shows that passing input points through a simple Fourier feature mapping enables an MLP to learn high-frequency functions in low-dimensional problem domains. It is worth noting that the seismic interpolation task with MLP relies on a low-dimensional problem as explained below.

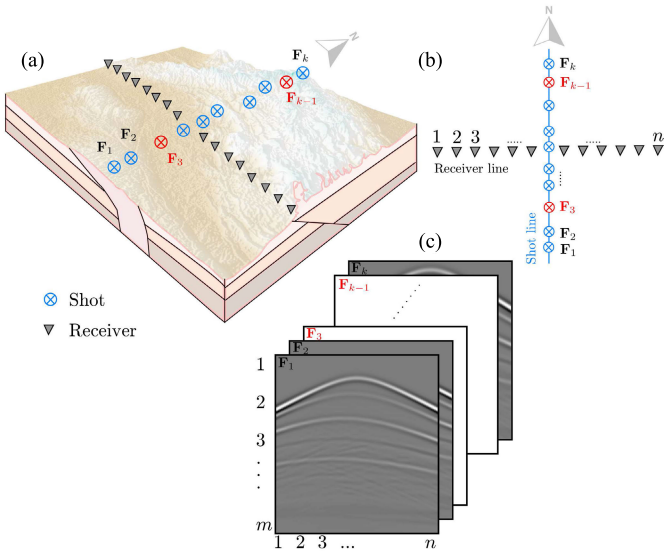

Fig. 1. Cross-spread geometry in irregular survey with missing shots $\mathbf{F}_3$ and $\mathbf{F}_{k-1}$ in red. (a) Perspective view. (b) Plan view and (c) seismic data in tensor representation $\mathcal{F}$.

III. 3-D Seismic Acquisition Model

Ideal seismic surveys are orthogonal grids with uniformly spaced receivers and sources (i.e., preplot design). In practice however, environmental and topographic restrictions induce irregularities that result in nonuniform spatial intervals, as illustrated by the cross-spread acquisition example in Fig. 1(a) and (b), where missing shots are depicted in red. Data from cross-spread surveys are modeled as cubes of k stacked shot gathers $\mathbf{F}_i \in \mathbb{R}^{m\times n}$, with m time samples and n receivers. Thus, the whole dataset can be denoted as a tensor $\mathcal{F} = \{\mathbf{F}_i\}_{i=1}^{k} \in \mathbb{R}^{m\times n\times k}$. Fig. 1(c) shows a survey with missing shot gathers $\mathbf{F}_3$ and $\mathbf{F}_{k-1}$. Letting $\mathbf{f} \in \mathbb{R}^{mnk}$ be the vector representation of the full cross-spread seismic survey $\mathcal{F}$, the acquisition model can be written as the linear system

$$\mathbf{r} = \mathbf{\Phi}\mathbf{f} + \omega \tag{1}$$

with $\mathbf{\Phi}$ as the matrix modeling the sampling process, ω the acquisition noise, and $\mathbf{r} \in \mathbb{R}^{mn(k-s)}$ is the incomplete acquired data (seismic response). Specifically, the acquisition operator $\mathbf{\Phi} \in \mathbb{R}^{mn(k-s)\times mnk}$ is defined as $\mathbf{\Phi} = \mathbf{S} \otimes \mathbf{I}_{mn}$, where $\otimes$ represents the Kronecker product [31], $\mathbf{I}_{mn}$ is an $mn \times mn$ identity matrix, and $\mathbf{S} \in \mathbb{R}^{k-s\times k}$ is an identity matrix modeling the subsampling effect by setting it to zero the s rows that correspond to the linear indices of the missing sources.

Previous works have shown that the underlying seismic data $\mathbf{f}$ can be estimated from the incomplete acquisition $\mathbf{y}$, following either optimization or data-driven approaches. Specifically, optimization methods consider that seismic signals are sparse in some transformation domain $\mathbf{\Psi}$, such that they can be represented as $\mathbf{\Psi}\mathbf{f} = \alpha$, where α corresponds to the coefficients

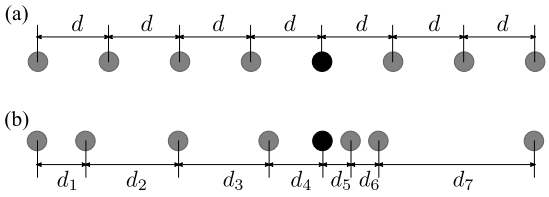

Fig. 2. Source sampling with (a) uniform and regular interval with distance d and (b) irregular interval with variable distance. Black dots represent missing shots to be interpolated.

in the transformed domain [2], [3], [5], [32], [33]. Using such a sparsity prior, it is possible to estimate $\mathbf{f}$ by solving the optimization problem given by

$$\mathbf{f}^* = \arg\min_{\mathbf{f}} \frac{1}{2}\|\mathbf{r} - \mathbf{\Phi}\mathbf{f}\|_2^2 + \lambda\|\mathbf{\Psi}\mathbf{f}\|_1 \tag{2}$$

where $\lambda > 0$ is a regularization parameter weighting the sparsity term in the solution. On the other hand, missing seismic data can be recovered using data-driven approaches, such as CNNs that learn internal structures of extensive seismic datasets [10], [11], [12]. Nonetheless, all these methods rely on the sensing matrix $\mathbf{\Phi}$, which accounts for indexed sampling positions. Thus, it assumes a regular sampling grid, as illustrated in Fig. 2(a), i.e., it cannot model irregularly-spaced sources. Therefore, reconstruction methods still face limitations in providing accurate seismic estimates for irregular surveys, as the one depicted in Fig. 2(b), where the distance between sources is not fixed.

To address this problem, Hennenfent et al. [34] incorporated a nonequispaced curvelet transform within a sparsity-promoting prior, and Galvis et al. [4] used interpolation operators on the irregular grid before applying reconstruction algorithms with a binning preprocessing step to cast the irregularly sampled data into a regular grid. The main drawback of these approaches is that the interpolator assumes linear continuity, since it is applied only in the shot direction, which in 3-D acquisitions does not allow interpolation of the 2-D wavefield. For this reason, the approach in [4] is limited to 2-D shots in split-spread geometries.

IV. Coordinate-Based Seismic Shot Interpolation

Unlike the state-of-the-art interpolation methods that rely on index-based modeling of the survey, the proposed CoBSI method employs a coordinate-based deep internal learning approach for modeling the seismic survey in a more realistic fashion. The core idea of the proposed approach is motivated by recent computational imaging works in neural interpolation [24], [25], [26], [29], [35], [36], and consists of representing the acquired response of the wavefield $r \in \mathbb{R}$ from a given coordinate $\boldsymbol{v} = [x, y, z] \in \mathbb{R}^3$, where x, y, z, respectively, denote the time, receiver, and source positions, with a neural network $\mathcal{M}_{\boldsymbol{\theta}}$ with parameters $\boldsymbol{\theta}$. The goal of this neural network is to map input coordinates to the sampled wavefield responses, i.e., $r = \mathcal{M}_{\boldsymbol{\theta}}(\boldsymbol{v})$. Based on this representation, we can model the acquired cross-spread $\mathbf{r}$ from (1) by querying $\mathcal{M}_{\boldsymbol{\theta}}$ using the corresponding coordinates of the acquired response (see Fig. 3).

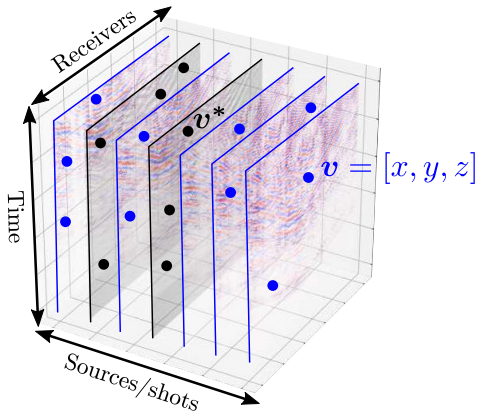

Fig. 3. Illustration of the coordinate-based representations $\boldsymbol{v}$ in a single cross-spread grid for seismic acquisition (blue dots), with x, y, z denoting receiver, time, and source coordinates, respectively. Coordinates $\boldsymbol{v}^*$ belong to the desired shot gathers to interpolate (black dots).

The proposed neural network $\mathcal{M}_{\boldsymbol{\theta}}$ is the composition of a high-dimensional mapping γ, and an MLP $\mathcal{N}_{\boldsymbol{\theta}}$ such that $\mathcal{M}_{\boldsymbol{\theta}}(\boldsymbol{v}) = \mathcal{N}_{\boldsymbol{\theta}}(\gamma(\boldsymbol{v}))$. Recent works have demonstrated that this separation mitigates the performance degradation observed in MLP to represent high-frequency variations [29], [35], [37], such as those measured in seismic data due to abrupt changes in the continuity of reflection events, or coherent noise such as body waves and ground roll. Sections IV-A and IV-B present the details of the mapping function γ and the MLP $\mathcal{N}_{\boldsymbol{\theta}}$ architecture.

A. Anisotropic Positional Encoding

To address the problem of representing high-frequency components of natural images, Tancik et al. [29] proposed to employ a positional encoding γ as high-dimensional mapping, given by

$$\gamma_U(\boldsymbol{v}) = [\cos(\omega_1\boldsymbol{v}), \sin(\omega_1\boldsymbol{v}), \ldots, \cos(\omega_i\boldsymbol{v}), \sin(\omega_i\boldsymbol{v}), \ldots, \cos(\omega_U\boldsymbol{v}), \sin(\omega_U\boldsymbol{v})]^T \tag{3}$$

where U is the total number of components, $\{\omega_i\}_{i=1}^{U}$, the frequency mappings are given by $\omega_i = i\pi/2$ or $\omega_i = \pi 2^{i-1}$ in the linear and exponential sampling, respectively, and $\boldsymbol{v}$ is some arbitrary coordinate normalized to lie in $[0, 1]^3$. Note that the positional encoding defined in (3) expands the input coordinates as the combination of different frequency components and, all coordinates are mapped to the same number of frequencies.

However, in the particular case of seismic data, each signal coordinate represents substantially different features (sources, receivers, and time samples), which should not be equally encoded to preserve the structure of the data. Therefore, this work proposes to employ an anisotropic positional encoding, in which a different number of frequency components is used for each axis direction. Thus, for the 3-D case of seismic data, the anisotropic positional encoding is defined as

$$\Gamma_{MNK}(\boldsymbol{v}) = [\gamma_M(x), \gamma_N(y), \gamma_K(z)]^T \tag{4}$$

where M, N, K are the number of frequency components associated with x (time), y (receiver), and z (shot) axes as

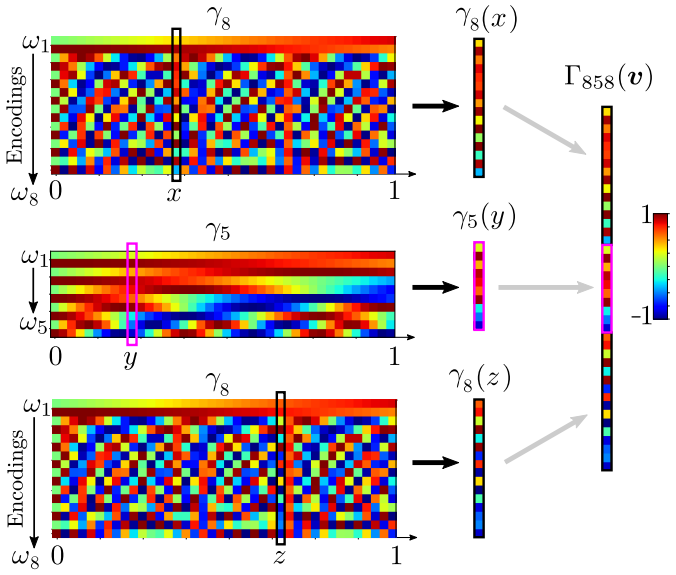

Fig. 4. Conceptual example of anisotropic positional encoding maps with linear sampling with $M = 8$, $N = 5$, and $K = 8$ number of frequencies. The matrices on the left represent the γ functions for each coordinate, respectively. The vectors in the middle represent the corresponding mapping for a given coordinate x, y, and z. Finally, the vector in the right $\Gamma_{858}(\boldsymbol{v})$ illustrates the final mapping of the proposed anisotropic positional encoding.

shown in Fig. 3. Fig. 4 illustrates an example of the anisotropic positional encoding for $M = 8$, $N = 5$, and $K = 8$, where the horizontal axis for all encoding maps represents the normalized coordinate values lying in $[0, 1]$, the vertical axis represents the number of encoding frequencies, and the output Γ lies in $[-1, 1]$. The number of frequency components for each coordinate M, N, K is found via parameter tuning.

B. Network Architecture

An MLP is here used to approximate the function $\mathcal{N}_\theta$. This architecture is modeled as the nested functions

$$\mathcal{N}_{\boldsymbol{\theta}}(\boldsymbol{v}) = f_L(f_{L-1}(\cdots f_2(f_1(\boldsymbol{v})))) \tag{5}$$

where L is the number of layers or depth of the MLP, and $f_i(\boldsymbol{v}_i) = \phi(\mathbf{W}_i\boldsymbol{v}_i + \mathbf{b}_i)$ is the i-th layer of the MLP, which is an affine transformation represented by the matrix $\mathbf{W}_i$ and bias $\mathbf{b}_i$, followed by a nonlinear activation function ϕ. This work adopts the rectified linear unit (ReLU) as activation function, which is one of the most widely employed in modern neural networks [38]. Moreover, since seismic data are normalized in the range $[0, 1]$, the sigmoid activation function has been selected for the output layer.

The overview of the proposed coordinate-based neural network is depicted in Fig. 5 with a fully connected block of NN neurons and L layers, and a single-neuron output layer. Note that it can be seen as a regression problem, such that we can simply employ a mean squared error (mse) loss function to find the optimal network parameters, $\boldsymbol{\theta}^*$. The mse loss function can be written as

$$\mathcal{L}(\boldsymbol{\theta}) = \frac{1}{mn(k-s)} \sum_{i}^{mn(k-s)} (r_i - \mathcal{N}_{\boldsymbol{\theta}}(\Gamma_{MNK}(\boldsymbol{v}_i)))^2 \tag{6}$$

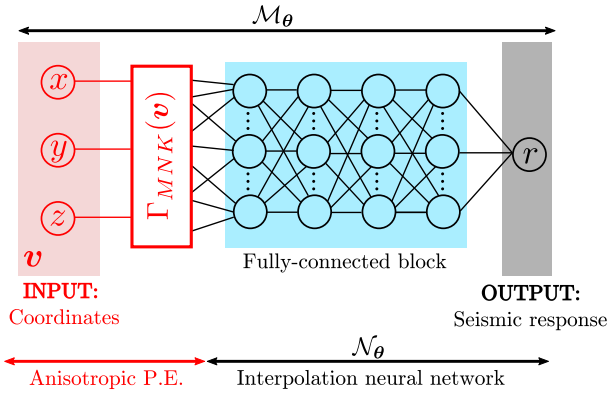

Fig. 5. Coordinate-based neural network $\mathcal{M}_{\boldsymbol{\theta}}$ with anisotropic positional encoding (P.E) and interpolation neural network $\mathcal{N}_{\boldsymbol{\theta}}$.

where s and k are the number of missing and total shots, respectively; $\boldsymbol{v}_i = [x_i, y_i, z_i]$ is the i-th element of the set of coordinates $\mathcal{V}$, and r_i is the ith entry of the acquired amplitude values $\mathbf{r}$ from (1).

We remark here that training data from additional seismic surveys are not necessary because we just employ the available discrete samples of the acquisition of interest for training the network.

C. Interpolation Algorithm

The anisotropic positional encoding and MLP from Sections IV-A and IV-B are combined as the CoBSI method described in Algorithm 1. Specifically, the inputs of the algorithm are given as follows.

1) The set of coordinates of the available (acquired) data $\mathcal{V} = \{\boldsymbol{v}_i\}_{i=1}^{mn(k-s)}$, with $\boldsymbol{v}_i = [x_i, y_i, z_i]$.
2) The corresponding amplitude values of the acquired data $\mathbf{r} = [r_1, \ldots, r_i, \ldots, r_{mn(k-s)}]$ from (1).
3) The set of coordinates of the missing data $\mathcal{V}^* = \{\boldsymbol{v}_i^*\}_{i=1}^{mns}$.

In step 1, the anisotropic positional encoding of each point $\boldsymbol{v}_i$ is calculated using (4). Then, in lines 3–10 the positional encodings and the amplitude values are used to train the MLP $\mathcal{N}_\theta$ in an end-to-end fashion, to obtain the optimized network parameters $\boldsymbol{\theta}^*$, as in step 11 of Algorithm 1. In lines 12–14, the network with optimal parameters is used to estimate the amplitude values of the missing shots by querying $\mathcal{M}_{\boldsymbol{\theta}}$, using the corresponding coordinates $\mathcal{V}^* = \{\boldsymbol{v}_i^*\}_{i=1}^{mns}$ of the s missing shot-gathers, as long as the input coordinates are in the same acquisition domain. Specifically, note that in terms of seismic surveys, the acquisition domain is related to the maximum coverage in the receiver and source lines as shown in Fig. 3. In line 15, these amplitudes are concatenated to the known data amplitudes, and rearranged as 2-D structures corresponding to the seismic shots (line 16). Thus, a full seismic data cube $\mathcal{F}$ is obtained.

V. Simulations and Results

Three different experiments were carried out to evaluate the effectiveness of CoBSI in regular and irregular cross-spread acquisition geometries, using synthetic and real data. In all the experiments, we fixed the number of layers of the MLP

Algorithm 1 Seismic Shot Interpolation Using CoBSI Method

Require: $\mathcal{V}$: Set of coordinates; $\mathbf{r}$: Data amplitude values corresponding to each coordinate. $\mathcal{V}^*$: Set of coordinates for the missing shots. N_E: Number of iterations.

Calculate set $\mathcal{P} = \{\Gamma_{MNK}(\boldsymbol{v}_i)\}_{i=1}^{mn(k-s)}$ using Eq. 4 and $\boldsymbol{v}_i \in \mathcal{V}$.
Initialize $\boldsymbol{\theta}$ randomly
for $i = 1 \ldots . N_E$ **do**
  Draw $\mathcal{P}_t \subset \mathcal{P}$, $\mathbf{r}_t$ from $\mathbf{r}$ ▷ Draw data batch
  for each $\Gamma_{MNK}(\boldsymbol{v}_j) \in \mathcal{P}_t$, $\mathbf{r}_j$ from $\mathbf{r}_t$ **do**
    $\hat{r}_j \leftarrow \mathcal{N}_\theta(\Gamma_{MNK}(\boldsymbol{v}_j))$ ▷ Estimate the seismic response
    Compute MSE loss $\mathcal{L}(\boldsymbol{\theta})$ using $\hat{r}_j, r_j$, and Eq. 6.
    Update $\boldsymbol{\theta}$ using ADAM optimizer
  end for
end for
Get the optimal parameter $\boldsymbol{\theta}^*$ from last iteration
for each $\boldsymbol{v}_i^* \in \mathcal{V}^*$ **do**
  $\hat{r}_i^* \leftarrow \mathcal{N}_{\boldsymbol{\theta}^*}(\Gamma_{MNK}(\boldsymbol{v}_i^*))$ ▷ Estimate the seismic responses for missing shots
end for
$\mathbf{f} \leftarrow [\hat{\mathbf{r}}^*, \mathbf{r}]$ ▷ Concatenate acquired and interpolated seismic response
$\mathcal{F} \in \mathbb{R}^{m \times n \times k} \leftarrow$ reshape($\mathbf{f} \in \mathbb{R}^{mnk}$) ▷ Rearrange vector to tensor representation
Output: $\mathcal{F}$ complete seismic data

TABLE I

SUMMARY OF PARAMETERS FOR THE COORDINATE-BASED NEURAL NETWORK $\mathcal{M}_\theta$ ON EACH EXPERIMENT. NN: NUMBER OF NEURONS, LR: LEARNING RATE, NTP: NUMBER OF TRAINABLE PARAMETERS

Experiment	Dataset	NN	LR	Epochs	NTP
I	Synthetic	128	1e-3	1000	232449
II	Stratton	256	1e-3	5000	932865
III	SEAM Phase II	128	1e-4	50000	234241

architecture to $L = 15$ with the same number of neurons (NN) per layer. Table I summarizes the main network parameters used for training on each experiment: dataset, NN, learning rate, epochs, and the number of trainable parameters (NTP). These parameters were found by grid search, so that the best peak signal-to-noise ratio (PSNR) metric was obtained on each experiment.

Particular details on each dataset and experiment are included in Sections V-A–V-C. All experiments were conducted using the NVIDIA Tesla P100 16-GB GPU. The PSNR is here used to assess the accuracy of the reconstructions, exactly as described by Liang et al. [39], as well as the structural similarity image metric (SSIM) from [40]. Both metrics were applied in the time-domain shots, with respect to the ground truth. Interpolated shots obtained with CoBSI are compared against those resulting from the F-XY domain MSSA and DMSSA method [41] with fhigh = 550 and iter = 50 implemented using the DRR MATLAB package [42], SGK using fast dictionary learning for high-dimensional seismic reconstruction [43], [44], and the sparsity-based interpolation (SBI) in (2), solved with the alternating direction method of multipliers (ADMM) algorithm from [3]. All the parameters in these methods were fixed to those suggested by the authors of each work.

TABLE II

INTERPOLATION RESULTS FOR FIVE MISSING SHOTS IN EXPERIMENT I, USING THE PROPOSED COBSI METHOD WITH EXPONENTIAL AND LINEAR SAMPLING (COBSI-EXP AND COBSI-LIN, RESPECTIVELY)

Shot	SSIM		PSNR (dB)	
	CoBSI-Exp	CoBSI-Lin	CoBSI-Exp	CoBSI-Lin
S4	0.990	0.987	42.368	42.701
S6	0.983	0.980	42.070	41.542
S8	0.977	0.969	36.859	34.767
S11	0.977	0.976	37.343	40.587
S13	0.980	0.977	37.479	36.707
Average	**0.982**	0.978	39.224	**39.261**
Std. Dev.	0.005	0.007	2.746	3.373

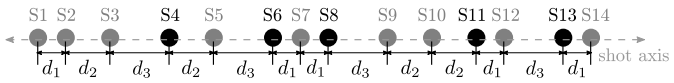

Fig. 6. Synthetic irregular shot acquisition employed in Experiment I, with $d_1 = 75$ m, $d_2 = 100$ m, and $d_3 = 125$ m. Black dots indicate missing shots.

A. Experiment I

A synthetic dataset of an irregular acquisition from a cross-spread grid using the acoustic forward modeling operator from DEVITO [45], [46] to propagate the seismic wavefield was used in this experiment. The cross-spread comprises $m = 900$ time samples, $n = 101$ receivers, and $k = 14$ shots. The interval samplings are $dt = 1$ ms, $dg = 25$ m, respectively, for time and receivers. For this experiment, five shots (S4, S6, S8, S11, and S13) were removed from the dataset, and interpolated using the proposed CoBSI method. Fig. 6 depicts the irregular interval in shot sampling, where the five missing shots are represented by black dots. Note that the removed shots account for different distance intervals among known data.

Besides evaluating the ability of CoBSI to interpolate seismic shots from a synthetic irregular dataset, this experiment aims at analyzing the behavior of linear and exponential frequency mappings in the anisotropic positional encoding. Table II summarizes the CoBSI interpolation metrics for the five missing shots. Specifically, as a result of parameter tuning, the number of frequencies was fixed at 1 for time and shots, and 2 for receivers, i.e., Γ_{121}. The attained results show small variations in the metrics obtained with the two types of sampling for the anisotropical positional encoding function. Fig. 7 presents the interpolation results of shot S6, which exhibits discontinued seismic events highlighted by the arrows, that are not fully interpolated by CoBSI with exponential sampling. On the other hand, with linear sampling, CoBSI is able to smooth the entire signal by estimating more continuous events throughout the shot.

Table III summarizes CoBSI-Exp interpolation results compared with those from DMSSA, MSSA SGK and SBI. It can be seen that the proposed approach outperforms the evaluated counterparts in both metrics. Fig. 8 shows that unlike the comparison methods, where most of the reconstruction errors occur in the reflection events, CoBSI shows a small distribution of

TABLE III

RESULTS SUMMARY FOR THE INTERPOLATED SHOTS OBTAINED WITH COBSI, COMPARED WITH RESPECT TO DMSSA, MSSA, SGK, AND SBI METHODS USING THREE DIFFERENT SEISMIC ACQUISITION SURVEYS

Experiment	Shot	SSIM					PSNR (dB)				
		CoBSI	DMSSA	MSSA	SGK	SBI	CoBSI	DMSSA	MSSA	SGK	SBI
Experiment I: **Synthetic**	S4	0.990	0.294	0.284	0.493	0.547	**42.368**	17.737	18.379	19.261	20.845
	S6	**0.983**	0.237	0.239	0.459	0.741	**42.070**	14.933	15.707	19.146	26.463
	S8	**0.977**	0.277	0.253	0.453	0.921	**36.589**	20.276	19.486	19.562	22.026
	S11	**0.977**	0.183	0.135	0.461	0.583	**37.343**	19.241	17.867	18.155	21.199
	S13	**0.980**	0.060	0.065	0.431	0.481	**37.479**	14.188	14.318	15.609	17.264
	Average	**0.981**	0.210	0.195	0.459	0.655	**39.170**	17.275	17.151	18.347	21.559
Experiment II: **Stratton 3D survey**	S3	**0.651**	0.084	0.070	0.435	0.503	**22.621**	15.419	14.850	16.510	17.371
	S6	**0.552**	0.106	0.092	0.402	0.520	**19.970**	15.412	14.900	16.098	19.233
	Average	**0.602**	0.095	0.081	0.419	0.512	**21.296**	15.416	14.875	16.304	18.302
Experiment III: **SEAM Phase II**	S2	**0.724**	0.150	0.083	0.399	0.296	**23.379**	17.398	15.416	18.082	20.195
	S4	**0.728**	0.255	0.185	0.436	0.229	**24.812**	19.768	18.154	19.183	19.807
	Average	**0.726**	0.203	0.134	0.418	0.263	**24.096**	18.583	16.785	18.633	20.001

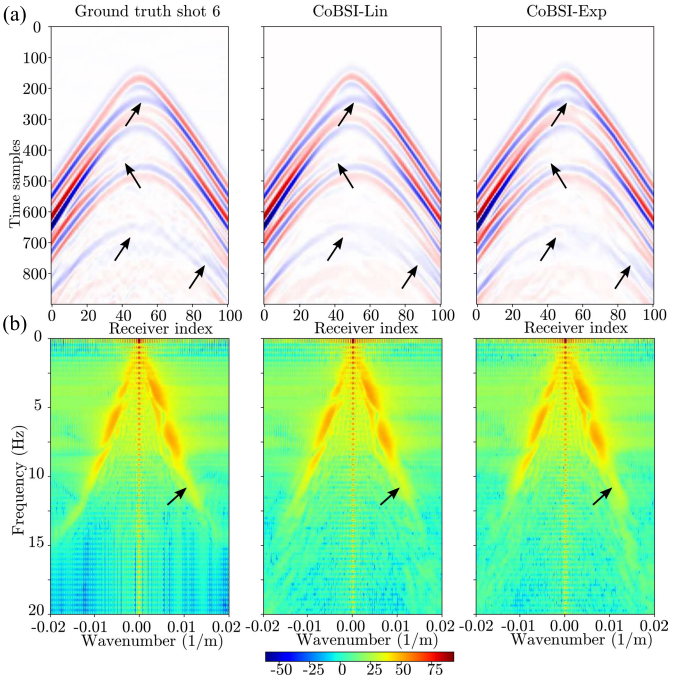

Fig. 7. Comparison between shot 6 interpolation using linear and exponential sampling in the positional encoding function for the experiment I in (a) time and (b) frequency-wavenumber domain. Arrows point at the main differences and correspond to events whose continuity is better approximated by CoBSI-Lin.

errors toward the edges of the shot gather, thus, exhibiting a high reconstruction accuracy in the first arrivals, as well as in linear and hyperbolic events. Moreover, considering the averaged results, CoBSI outperforms the comparative methods by up to 0.786 (SSIM) and 22.018 dB (PSNR).

In an attempt to provide some insight into the function of the neural network, we used a set of coordinates, regularly sampled in the interval $[0, 1]$ along the receiver and time dimensions (101 and 900 samples, respectively), and fixed the source coordinate at $z = 0.5$, to plot the outputs of a single (arbitrary) neuron for each layer, as illustrated in Fig. 9. It can be noted that the first six layers resemble low-level features related to the overall structure of the location of first arrivals and the regions where reflections occur, while layers 8–15 approximate high-level features specifically associated with nonlinear seismic events, high-frequency structures, and overall improvement in the representation of delayed events. This evolution of the reconstructed characteristics in the hidden layers demonstrates the network's ability to interpolate the main seismic features based solely on irregular data measurements.

B. Experiment II

The seismic dataset employed for this experiment is the *Stratton survey* [27], a real 3-D land swath acquisition project from South Texas, which was rearranged as a cross-spread using a geometric analysis based on the survey characteristics. A subset of 1001 time samples, 90 receivers, and ten sources, with a gap between the fifth and sixth shots, as illustrated in Fig. 10. The goal of this experiment is to evaluate the ability of the proposed method to deal with real more complex data. To this end, we removed shots S3 and S6, such that two different gap lengths are considered. The interpolation challenge in these real data is to determine the correct position of the seismic reflection event in the vertical axis (time axis). In this case, the number of frequencies for the positional encoding was fixed at 9 for the time axis, 5 for receivers, and 8 for shots, i.e., Γ_{958}.

Fig. 11 presents a comparison between the interpolation results for shot S6, where it can be seen that the interpolated signals are smoother and more continuous than the ground truth, which explains the resulting lower metric values. These results show that the main advantage provided by CoBSI with Γ_{958} in linear sampling is that it can preserve the polarities and location of events on the time axis, pointed by arrows.

For instance, SBI fails in interpolating the events signaled by arrows in Fig. 11, located close to receiver index 25 and in the time samples 300 and 500, respectively, because it does not have enough neighboring shot information to estimate the correct temporal position of the events. Moreover, CoBSI provides a stronger denoised signal enhancing and highlighting the seismic events in the shot. As in the previous case, the results for Experiment II in Table III show that CoBSI-Exp interpolation provides more accurate results compared to DMSSA, MSSA SGK, and SBI, for both met-

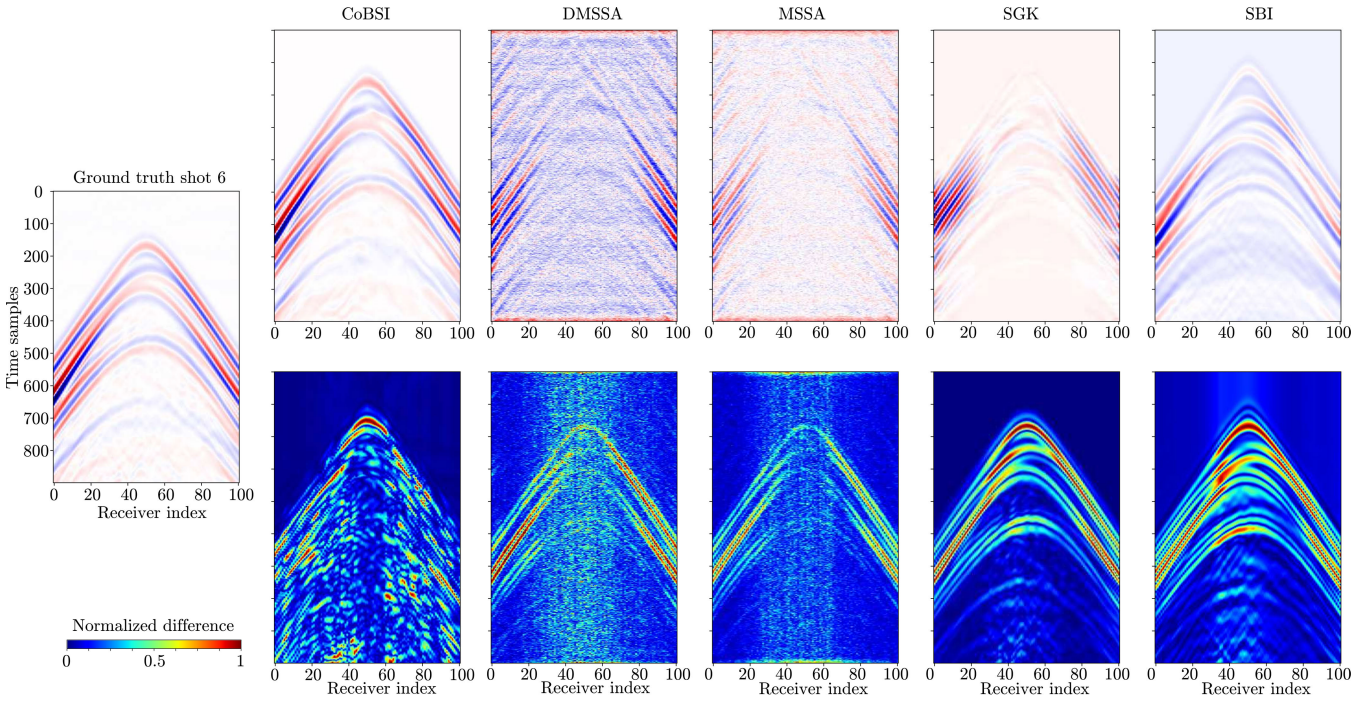

Fig. 8. Comparison of shot 6 interpolation results from Experiment I using CoBSI, DMSSA, MSSA, SGK, and SBI methods.

rics. The improvements in this experiment go up to 0.521 (SSIM) and 6.421 dB (PSNR), for the averaged results of all shots.

C. Experiment III

The dataset used in this experiment is a part of the *SEAM Phase II Foothills model*. The acquisition is an orthogonal survey over a complex geological model simulating the Llanos Foothills of the Andes Mountains in Colombia, one of the most challenging regions of active land exploration [28], mainly because of complex seismic events with abrupt changes in amplitude caused by the topography. The dataset comprises $m = 128$ time samples, $n = 128$ receivers, and $k = 7$ shots. The interval samplings are $dt = 8$ ms, $dg = 50$ m, and $ds = 50$ m for time, receivers, and shots, respectively. In this experiment, we evaluate the performance of CoBSI in regular acquisitions. Thus, shots S2 and S4 were removed from the survey, and the interpolated shots are illustrated in Fig. 12. It can be seen that CoBSI with Γ_{551} in linear sampling reconstructs the events preserving the tilt and polarities, while SBI method yields events with low amplitude, as well as artifacts in the main reflection events located in the center of the shot. Further, due to the complexity of the distribution of the reflection events, the competing interpolation methods fail in correctly reconstructing the low amplitude signals, this can be seen in the error images, with larger error values distributed throughout the shot, while in CoBSI the errors occur mostly at the bottom of the shot gather. Therefore, in this scenario, CoBSI exhibits higher accuracy as it is able to highlight the main seismic reflection events in the shot gathers. The results for this experiment in Table III verify this behavior with gains of up to 0.592 (SSIM) and 7.311 dB (PSNR) in the average results.

VI. Discussion

In general, the previous results demonstrate that CoBSI interpolation outperforms DMSSA, MSSA SGK and SBI for all experiments, providing adequate representations of the typical characteristics of a seismic shot such as smoothness and continuity in the events, noise reduction, and amplitude compensation. Sections VI-A and VI-B discuss the advantages and limitations of CoBSI related to seismic neural representation and computational costs.

A. Seismic Neural Representation

This work aims to show that a complete and continuous representation of seismic data can be obtained by coupling the anisotropic positional encoding and the MLP, despite the simplicity of the neural network, as it has been previously shown for other computational imaging problems [26], [35]. Further, it should be noted that the CoBSI formulation is flexible, so that other, more complex neural network architectures can be employed instead of the MLP, at the expense of their inherent computational complexity. One of the main advantages of CoBSI is that once the seismic neural representation is obtained from the available incomplete data, it is possible to estimate the response of the continuous field at any arbitrary coordinate within the analysis domain, so that complete missing shot gathers can be accurately estimated. In addition, compared to other interpolation or reconstruction methods where parameter tuning must be done, in CoBSI the number of frequencies in the mapping function is closely related to the dimensionality of the seismic data. Therefore, the hyperparameters M, N, K from (4) can be found by analyzing the type of seismic acquisition survey. Specifically, with few seismic sources in a cross-spread

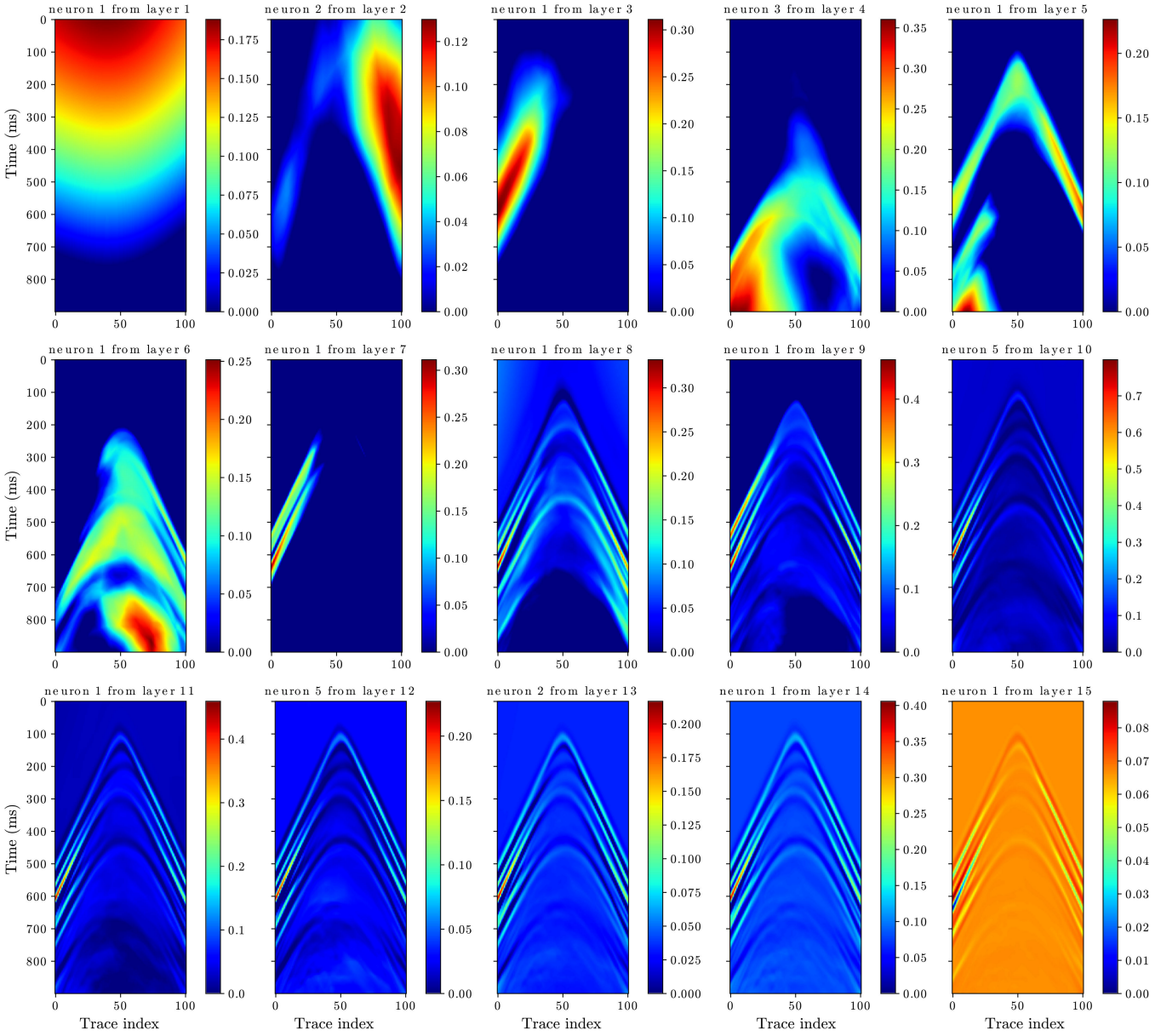

Fig. 9. Output features of 15 arbitrary neurons along different hidden layers for coordinates regularly sampled in the interval [0, 1] along the receiver and time dimensions (101 and 900 samples, respectively), and fixed source coordinate at $z = 0.5$.

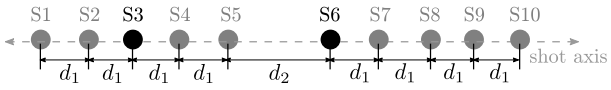

Fig. 10. Irregular real seismic acquisition employed in Experiment II, with $d_1 = 50$ m, $d_2 = 100$ m. Black dots indicate missing shots.

array, the signal variation will be mainly focused in the receiver direction (inline), because more spatial information exists. On the other hand, dealing with inline-offset spread or marine data, where the density of shots is high, the greatest variation of the signal occurs in the source direction (crossline).

B. Computational Cost

As shown in Table I, there are fewer than one million trainable parameters in CoBSI. To provide a comparison with respect to more complex network architectures employed in seismic reconstruction, Table IV presents the NTP of CNNs such as U-Net [23], [47] and autoencoders [48], [49], [50] under supervised learning schemes, as well as an ordinary CNN [36]. It is worth noting that these methods

TABLE IV
COMPARISON OF THE NTP REQUIRED IN SEISMIC RECONSTRUCTION METHODS

Seismic Data	Network	NTP	Learning
2D [23]	U-NET	87M	Supervised
2D [36]	CNN ordinary	42K	Unsupervised
3D [47]	U-NET	27M	Supervised
2D [48]	Autoencoder	18M	Supervised
3D [50]	Autoencoder	6M	Supervised
Shotgather (i.e. 3D)	CoBSI (MLP)	$<$1M	Unsupervised

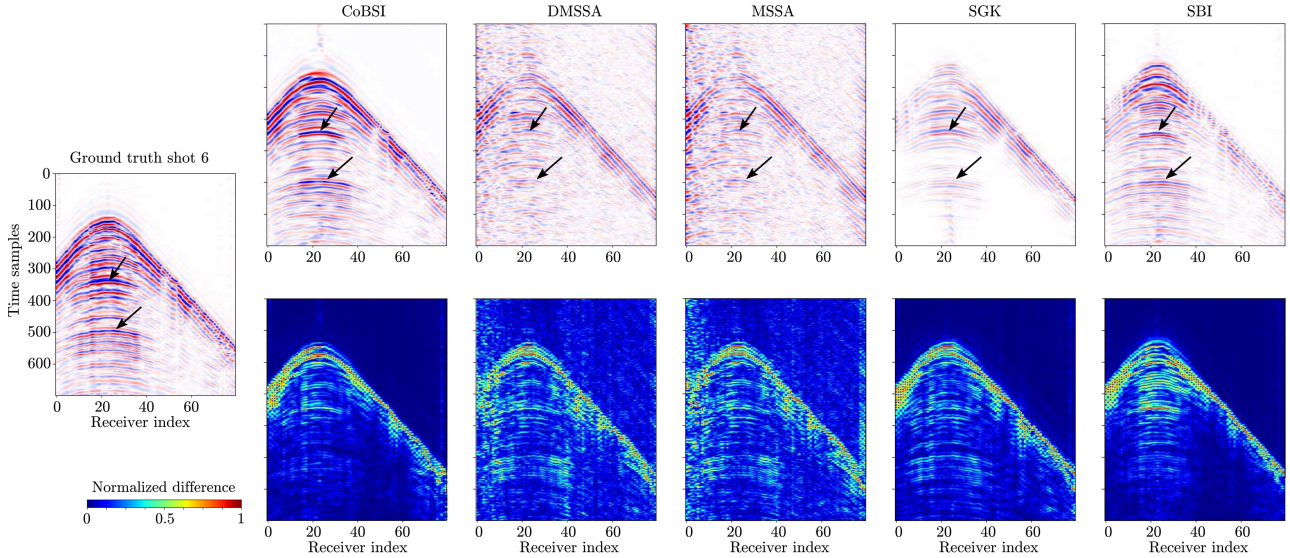

Fig. 11. Interpolation results for shot S6 from Experiment II, using CoBSI, DMSSA, MSSA, SGK, and SBI methods. The arrows point to the main seismic reflection events.

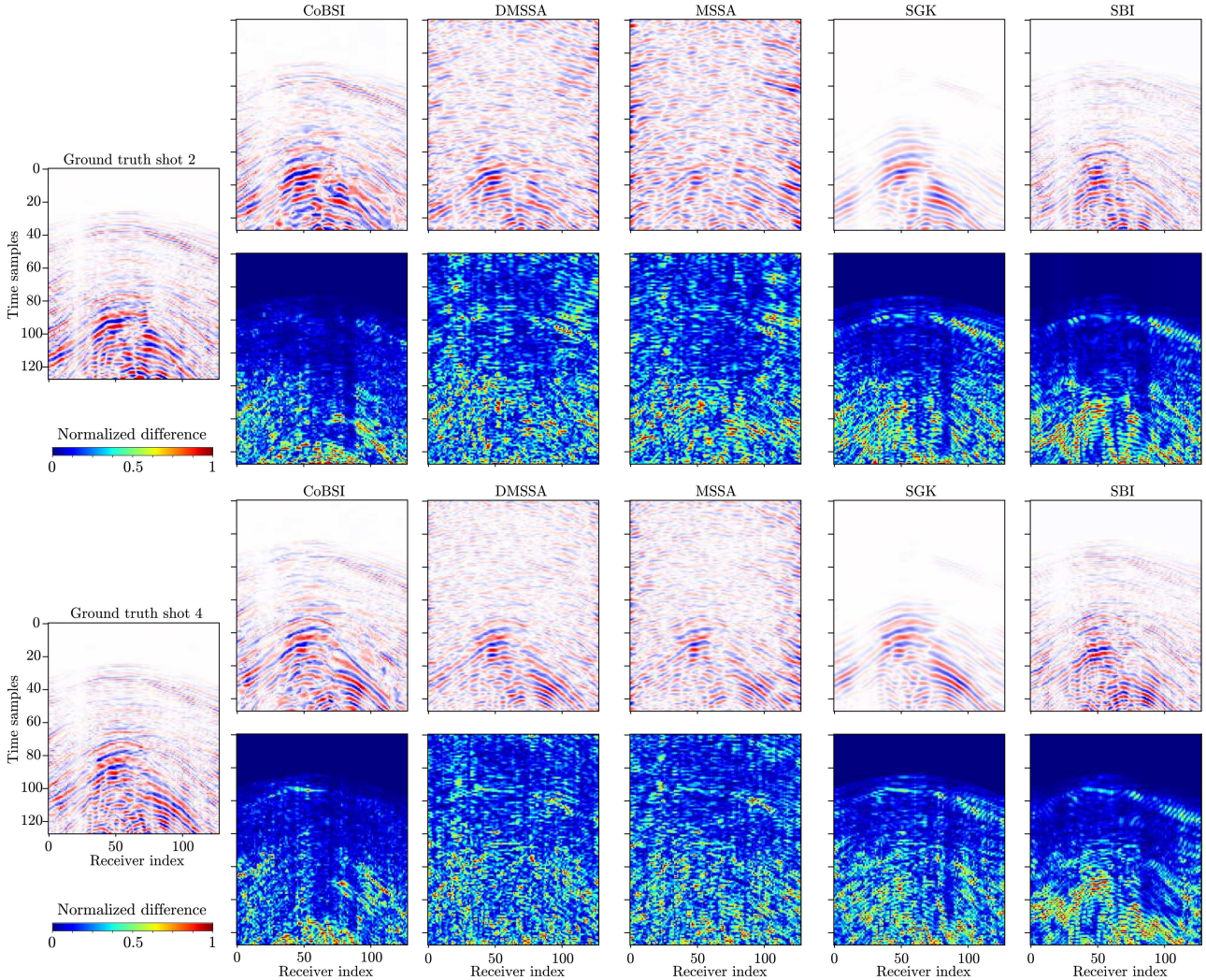

Fig. 12. SEAM Phase II data interpolation results for shots S2 and S4 from Experiment III, using CoBSI, DMSSA, MSSA, SGK, and SBI methods. Arrows point at events better approximated by CoBSI, while sparsity yields low amplitude events and artifacts in the main reflection events at the center of the shot.

focus on interpolating receivers in 2-D and 3-D seismic data. In contrast, CoBSI aims to estimate complete missing shots, which is substantially a more complex task. Further, it is able to obtain such interpolations employing a simpler network (MLP), entailing less computational resources in an unsupervised strategy, as only the weights and biases of the MLP are learned. While [36] is an unsupervised learning approach, it only considers missing trace reconstruction

for uniform subsampling, which is unrealistic for field applications.

A potential limitation of CoBSI, however, lies in the fact that it requires training an MLP for each new seismic dataset. Although the computer vision community has devoted a great deal of attention to reducing the cost of training implicit representations from scratch, by using previous knowledge of the underlying class of signals being represented [51], [52], [53], [54], this is still an active ongoing area of research that can be explored in future work.

Network parameter configuration is still required in CoBSI, as the MLP requires two configuration parameters, i.e., number of layers and NN per layer. Conducted experiments show that 15 layers are enough to represent all the analyzed datasets, with different complexity levels, and only the NN per layer has to be found by parameter tuning.

VII. Conclusion

A CoBSI method to estimate missing seismic shots in both regular and irregular 3-D land seismic acquisitions has been proposed. Unlike the state-of-the-art reconstruction methods that employ index-based models, CoBSI employs a coordinate-based approach that allows data interpolation in irregular geometries. Further, a key component of CoBSI is an anisotropic positional encoding layer in the neural network to map from low- to high-dimensional coordinates to consider the variation in the reference axes corresponding to time, receivers, and shots domains. Experimental results showed the ability of the proposed method on three different scenarios: 1) irregular geometry and synthetic wavefield; 2) geometry with a gap in real acquisition from Texas; and 3) the well-known geophysical *SEAM Phase II Foothills Model* with a regular acquisition. The obtained results demonstrated the advantages of the proposed method with respect to SBI and low-rank interpolation, since CoBSI can estimate continuous seismic events while providing a smooth signal in the space-time domains. Quantitatively, on average CoBSI outperformed the competing methods by up to 22.11 dB of PSNR in synthetic data and 6.4 and 7.31 dB for the real-data experiments.

Acknowledgment

The authors thank the Centre for High-Performance Computing (GUANE-UIS) and NVIDIA Academic Hardware Grant Program for providing computational resources to run the parameter tuning experiments.

References

[1] A. Cordsen, M. Galbraith, and J. Peirce, *Planning Land 3-D Seismic Surveys*. Houston, TX, USA: Society of Exploration Geophysicists, Jan. 2000.

[2] O. P. Villarreal, K. León, D. Espinosa, W. Agudelo, and H. Arguello, "Compressive sensing seismic acquisition by using regular sampling in an orthogonal grid," in *Proc. IEEE 7th Int. Workshop Comput. Adv. Multi-Sensor Adapt. Process. (CAMSAP)*, Dec. 2017, pp. 1–5.

[3] O. Villarreal, K. León-López, D. Espinosa, W. Agudelo, and H. Arguello, "Seismic source reconstruction in an orthogonal geometry based on local and non-local information in the time slice domain," *J. Appl. Geophys.*, vol. 170, Nov. 2019, Art. no. 103846.

[4] L. Galvis, J. M. Ramírez, E. Vargas, O. Villarreal, W. Agudelo, and H. Arguello, "Reconstruction of 2D seismic wavefields from nonuniformly sampled sources," *Electron. Imag.*, vol. 32, no. 14, p. 307, Jan. 2020.

[5] P. Goyes-Peñafiel, E. Vargas, C. V. Correa, W. Agudelo, B. Wohlberg, and H. Arguello, "A consensus equilibrium approach for 3-D land seismic shots recovery," *IEEE Geosci. Remote Sens. Lett.*, vol. 19, pp. 1–5, 2022.

[6] S. V. Venkatakrishnan, C. A. Bouman, and B. Wohlberg, "Plug-and-Play priors for model based reconstruction," in *Proc. IEEE Global Conf. Signal Inf. Process.*, Dec. 2013, pp. 945–948.

[7] U. S. Kamilov, C. B. Bouman, G. T. Buzzard, and B. Wohlberg, "Plug-and-play methods for integrating physical and learned models in computational imaging," *IEEE Signal Process. Mag.*, 2022.

[8] G. T. Buzzard, S. H. Chan, S. Sreehari, and C. A. Bouman, "Plug-and-play unplugged: Optimization-free reconstruction using consensus equilibrium," *SIAM J. Imag. Sci.*, vol. 11, no. 3, pp. 2001–2020, Jan. 2018.

[9] B. Wang, N. Zhang, W. Lu, J. Geng, and X. Huang, "Intelligent missing shots' reconstruction using the spatial reciprocity of Green's function based on deep learning," *IEEE Trans. Geosci. Remote Sens.*, vol. 58, no. 3, pp. 1587–1597, Mar. 2020.

[10] Y. Wang, B. Wang, N. Tu, and J. Geng, "Seismic trace interpolation for irregularly spatial sampled data using convolutional autoencoder," *Geophysics*, vol. 85, no. 2, pp. V119–V130, Mar. 2020.

[11] Q. Liu, L. Fu, and M. Zhang, "Deep-seismic-prior-based reconstruction of seismic data using convolutional neural networks," *Geophysics*, vol. 86, no. 2, pp. V131–V142, Mar. 2021.

[12] B. Wang, N. Zhang, W. Lu, and J. Wang, "Deep-learning-based seismic data interpolation: A preliminary result," *Geophysics*, vol. 84, no. 1, pp. V11–V20, Jan. 2019.

[13] W. Fang, L. Fu, M. Zhang, and Z. Li, "Seismic data interpolation based on U-Net with texture loss," *Geophysics*, vol. 86, no. 1, pp. V41–V54, Jan. 2021.

[14] H. Zhang, X. Yang, and J. Ma, "Can learning from natural image denoising be used for seismic data interpolation?" *Geophysics*, vol. 85, no. 4, pp. WA115–WA136, Jul. 2020.

[15] H. Zhang, L. Mai, H. Jin, Z. Wang, N. Xu, and J. Collomosse, "An internal learning approach to video inpainting," in *Proc. IEEE/CVF Int. Conf. Comput. Vis. (ICCV)*, Oct. 2019, pp. 2720–2729.

[16] A. Shocher, N. Cohen, and M. Irani, "Zero-shot super-resolution using deep internal learning," in *Proc. IEEE/CVF Conf. Comput. Vis. Pattern Recognit.*, Jun. 2018, pp. 3118–3126.

[17] O. M. Saad, S. Fomel, R. Abma, and Y. Chen, "Unsupervised deep learning for 3D interpolation of highly incomplete data," *Geophysics*, vol. 88, no. 1, pp. WA189–WA200, Jan. 2023.

[18] M. J. Park, J. Jennings, B. Clapp, and B. Biondi, "Seismic data interpolation using a POCS-guided deep image prior," in *Proc. SEG Tech. Program Expanded Abstr.*, Sep. 2020, pp. 3154–3158.

[19] F. Kong, F. Picetti, V. Lipari, P. Bestagini, X. Tang, and S. Tubaro, "Deep prior-based unsupervised reconstruction of irregularly sampled seismic data," *IEEE Geosci. Remote Sens. Lett.*, vol. 19, pp. 1–5, 2022.

[20] D. Yoon, Z. Yeeh, and J. Byun, "Seismic data reconstruction using deep bidirectional long short-term memory with skip connections," *IEEE Geosci. Remote Sens. Lett.*, vol. 18, no. 7, pp. 1298–1302, Jul. 2021.

[21] Q. Wang, L. Fu, S. Ruan, B. Chen, and H. Li, "Reconstructing seismic data by incorporating deep external and internal learning," *Explor. Geophys.*, vol. 53, no. 6, pp. 634–653, Nov. 2022.

[22] S. Mandelli, V. Lipari, P. Bestagini, and S. Tubaro, "Interpolation and denoising of seismic data using convolutional neural networks," 2019, *arXiv:1901.07927*.

[23] X. Chai, H. Gu, F. Li, H. Duan, X. Hu, and K. Lin, "Deep learning for irregularly and regularly missing data reconstruction," *Sci. Rep.*, vol. 10, no. 1, p. 3302, 2020.

[24] Y. Sun, J. Liu, M. Xie, B. Wohlberg, and U. S. Kamilov, "CoIL: Coordinate-based internal learning for tomographic imaging," *IEEE Trans. Comput. Imag.*, vol. 7, pp. 1400–1412, 2021.

[25] V. Sitzmann, J. Martel, A. Bergman, D. Lindell, and G. Wetzstein, "Implicit neural representations with periodic activation functions," in *Proc. Adv. Neural Inf. Process. Syst.*, vol. 33, 2020, pp. 7462–7473.

[26] B. Mildenhall, P. P. Srinivasan, M. Tancik, J. T. Barron, R. Ramamoorthi, and R. Ng, "NeRF: Representing scenes as neural radiance fields for view synthesis," *Commun. ACM*, vol. 65, no. 1, pp. 99–106, Jan. 2022.

[27] B. Hardage and S. Tinker. (2021) *Stratton 3D Survey*. Accessed: Jan. 29, 2021. [Online]. Available: https://dataunderground.org/no/dataset/stratton

[28] C. Regone, J. Stefani, P. Wang, C. Gerea, G. Gonzalez, and M. Oristaglio, "Geologic model building in SEAM phase II—Land seismic challenges," *Lead. Edge*, vol. 36, no. 9, pp. 738–749, Sep. 2017.

[29] M. Tancik et al., "Fourier features let networks learn high frequency functions in low dimensional domains," in *Proc. Adv. Neural Inf. Process. Syst.*, vol. 33, 2020, pp. 7537–7547.

[30] J. Zheng, S. Ramasinghe, and S. Lucey, "Rethinking positional encoding," 2021, *arXiv:2107.02561*.

[31] H. Zhang and F. Ding, "On the Kronecker products and their applications," *J. Appl. Math.*, vol. 2013, pp. 1–8, Jan. 2013.

[32] F. J. Herrmann and X. Li, "Efficient least-squares imaging with sparsity promotion and compressive sensing," *Geophys. Prospecting*, vol. 60, no. 4, pp. 696–712, Jul. 2012.

[33] C. Li, C. C. Mosher, and S. T. Kaplan, "Interpolated compressive sensing for seismic data reconstruction," in *Proc. SEG Tech. Program Expanded Abstr.*, Sep. 2012, pp. 3274–3279.

[34] G. Hennenfent, L. Fenelon, and F. J. Herrmann, "Nonequispaced curvelet transform for seismic data reconstruction: A sparsity-promoting approach," *Geophysics*, vol. 75, no. 6, pp. WB203–WB210, Nov. 2010.

[35] J. T. Barron, B. Mildenhall, M. Tancik, P. Hedman, R. Martin-Brualla, and P. P. Srinivasan, "Mip-NeRF: A multiscale representation for anti-aliasing neural radiance fields," in *Proc. IEEE/CVF Int. Conf. Comput. Vis. (ICCV)*, Oct. 2021, pp. 5835–5844.

[36] Q. Wang, Y. Shen, L. Fu, and H. Li, "Seismic data interpolation using deep internal learning," *Explor. Geophys.*, vol. 51, no. 6, pp. 683–697, Nov. 2020.

[37] H.-M. Sun, R.-S. Jia, X.-L. Zhang, Y.-J. Peng, and X.-M. Lu, "Reconstruction of missing seismic traces based on sparse dictionary learning and the optimization of measurement matrices," *J. Petroleum Sci. Eng.*, vol. 175, pp. 719–727, Apr. 2019.

[38] V. Nair and G. E. Hinton, "Rectified linear units improve restricted Boltzmann machines," in *Proc. ICML*, 2010, pp. 1–11.

[39] J. Liang, J. Ma, and X. Zhang, "Seismic data restoration via data-driven tight frame," *Geophysics*, vol. 79, no. 3, pp. V65–V74, May 2014.

[40] Z. Wang, A. C. Bovik, H. R. Sheikh, and E. P. Simoncelli, "Image quality assessment: From error visibility to structural similarity," *IEEE Trans. Image Process.*, vol. 13, no. 4, pp. 600–612, Apr. 2004.

[41] W. Huang, R. Wang, Y. Chen, H. Li, and S. Gan, "Damped multichannel singular spectrum analysis for 3D random noise attenuation," *Geophysics*, vol. 81, no. 4, pp. V261–V270, Jul. 2016.

[42] Y. Chen, W. Huang, D. Zhang, and W. Chen, "An open-source MATLAB code package for improved rank-reduction 3D seismic data denoising and reconstruction," *Comput. Geosci.*, vol. 95, pp. 59–66, Oct. 2016.

[43] Y. Chen, "Fast dictionary learning for noise attenuation of multidimensional seismic data," *Geophys. J. Int.*, vol. 222, no. 3, pp. 1717–1727, Sep. 2020.

[44] H. Wang, W. Chen, Q. Zhang, X. Liu, S. Zu, and Y. Chen, "Fast dictionary learning for high-dimensional seismic reconstruction," *IEEE Trans. Geosci. Remote Sens.*, vol. 59, no. 8, pp. 7098–7108, Aug. 2021.

[45] M. Louboutin et al., "Devito (v3.1.0): An embedded domain-specific language for finite differences and geophysical exploration," *Geosci. Model Develop.*, vol. 12, no. 3, pp. 1165–1187, Mar. 2019.

[46] F. Luporini et al., "Architecture and performance of Devito, a system for automated stencil computation," *ACM Trans. Math. Softw.*, vol. 46, no. 1, pp. 1–28, Apr. 2020, doi: 10.1145/3374916.

[47] X. Chai, G. Tang, S. Wang, K. Lin, and R. Peng, "Deep learning for irregularly and regularly missing 3-D data reconstruction," *IEEE Trans. Geosci. Remote Sens.*, vol. 59, no. 7, pp. 6244–6265, Jul. 2021.

[48] S. Mandelli, F. Borra, V. Lipari, P. Bestagini, A. Sarti, and S. Tubaro, "Seismic data interpolation through convolutional autoencoder," in *SEG Technical Program Expanded Abstracts*. Houston, TX, USA: Society of Exploration Geophysicists, Aug. 2018, pp. 4101–4105.

[49] W. Xu, Y. Zhou, D. Liu, X. Wang, and W. Chen, "Seismic intelligent deblending via plug and play method with blended CSGs trained deep CNN Gaussian denoiser," *IEEE Trans. Geosci. Remote Sens.*, vol. 60, 2022, Art. no. 5913413.

[50] F. Qian, Z. Liu, Y. Wang, S. Liao, S. Pan, and G. Hu, "DTAE: Deep tensor autoencoder for 3-D seismic data interpolation," *IEEE Trans. Geosci. Remote Sens.*, vol. 60, 2022, Art. no. 5904219.

[51] M. Tancik et al., "Learned initializations for optimizing coordinate-based neural representations," in *Proc. IEEE/CVF Conf. Comput. Vis. Pattern Recognit. (CVPR)*, Jun. 2021, pp. 2845–2854.

[52] H. Yang et al., "ContraNeRF: Generalizable neural radiance fields for synthetic-to-real novel view synthesis via contrastive learning," in *Proc. IEEE/CVF Conf. Comput. Vis. Pattern Recognit.*, 2023, pp. 16508–16517.

[53] A. Yu, V. Ye, M. Tancik, and A. Kanazawa, "PixelNeRF: Neural radiance fields from one or few images," in *Proc. IEEE/CVF Conf. Comput. Vis. Pattern Recognit. (CVPR)*, Jun. 2021, pp. 4576–4585.

[54] M. M. Johari, Y. Lepoittevin, and F. Fleuret, "GeoNeRF: Generalizing NeRF with geometry priors," in *Proc. IEEE/CVF Conf. Comput. Vis. Pattern Recognit. (CVPR)*, Jun. 2022, pp. 18344–18347.